energies

MDPI

Article

A Calibration Procedure for an Analytical Wake Model Using Wind Farm Operational Data

Jian Teng [1,2] and Corey D. Markfort [1,2,3,*]

1 Mechanical Engineering, The University of Iowa, Iowa City, IA 52242, USA; jian-teng@uiowa.edu
2 IIHR-Hydroscience and Engineering, The University of Iowa, Iowa City, IA 52242, USA
3 Civil and Environmental Engineering, The University of Iowa, Iowa City, IA 52242, USA
* Correspondence: corey-markfort@uiowa.edu; Tel.: +1-319-335-6168

Received: 30 May 2020; Accepted: 3 July 2020; Published: 9 July 2020



Abstract: Wind energy is one of the fastest growing renewable energy sources in the U.S. Wind turbine wakes change the flow field within wind farms and reduce power generation. Prior research has used experimental and computational methods to investigate and model wind farm wake effects. However, these methods are costly and time-consuming to use commercially. In contrast, a simple analytical approach can provide reasonably accurate estimates of wake effects on flow and power. To reducing errors in wake modeling, one must calibrate the model based on a specific wind farm setting. The purpose of this research is to develop a calibration procedure for wind farm wake modeling using a simple analytical approach and wind turbine operational data obtained from the Supervisory Control And Data Acquisition (SCADA) system. The proposed procedure uses a Gaussian-based analytical wake model and wake superposition model. The wake growth rate varies across the wind farm based on the local streamwise turbulence intensity. The wake model was calibrated by implementing the proposed procedure with turbine pairs within the wind farm. The performance of the model was validated at an onshore wind farm in Iowa, USA. The results were compared with the industry standard wind farm wake model and shown to result in an approximate 1% improvement in sitewide total power prediction. This new SCADA-based calibration procedure is useful for real-time wind farm operational optimization.

Keywords: wind energy; wake modeling; wind farm optimization; analytical wake model; power prediction

1. Introduction

Wind energy is a mainstream source of electricity and continues to grow in usage to meet the future energy demands while reducing carbon emissions. At the end of 2019, the U.S. reached 105 GW wind energy capacity and continues to grow with 9143 MW capacity added in 2019 [1]. The U.S. now aims to generate 20% of the nation's electricity by 2030 and 35% by 2050 with wind energy [2]. More scientific research is needed to optimize wind farm and operation to meet the global demand for clean energy [3]. Wind turbine wakes, which reduce wind speed, are an important and ongoing challenge of wind energy research [4]. Turbine wakes are responsible for the change of flow field within a wind farm that affects the local climate and reduces power generation [3]. The effect of wind turbine wakes has been studied extensively using numerical, experimental, and analytical methods [5,6]. Although numerical and experimental studies can provide an accurate result in predicting the velocity and power deficit of the turbine arrays, they are costly and time-consuming. Analytical methods provide a simple, fast, and low-cost approach to model wind turbine wakes [5,7]. For these reasons, industry favors the analytical method for wind farm optimization [8].

Until now, there are many types of analytical wake models, such as the Jensen model [9,10], the Larsen model [11], and the Frandsen model [12]. The most commonly used wake model in the industry is still the Jensen wake model, which was developed in the early 1980s and assumed a top-hat distribution in the wake region [9,10]. This model has been extensively used in commercial software for wind farm planning or design, such as WAsP, Wind Farmer, and OpenWind [8]. The Jensen model is simplified by only considering the conservation of mass and does not consider the conservation of momentum [13]. While known for its simplicity and its ability to represent a realistic wake, the Jensen model has the disadvantage of overestimating the wake deficit in the far-wake region [14,15].

Recent studies, using both experimental [16] and numerical [17] experiments, revealed the velocity distribution is better represented by a self-similar Gaussian wake profile. Bastankhah and Porté-Agel proposed an analytical wake model that assumes a Gaussian shape in the far-wake region that applies both mass and momentum conservation [13]. To calculate the velocity deficit, the model requires an accurate determination of the wake growth rate and an estimation of the thrust coefficient. This model has been validated based on field measurements at a utility-scale wind turbine [18].

A recent study by Niayifar and Porté-Agel demonstrated that the new model can represent turbine wakes and power losses in an uniform layout offshore wind farm, Horns Rev [15]. The Horns Rev offshore wind farm has a regularly spaced wind turbine and exhibits a significant power deficit on actual measurements [19]. Unlike regularly spaced offshore wind farms, many onshore wind farms, especially in the US, have irregularly spaced layouts. The power deficit at these wind farms may not be as significant as observed at the Horns Rev wind farm. Niayifar and Porté-Agel's study calibrated the analytical model's parameters with the numerical data generated from the Large Eddy Simulation (LES). The results were also compared against the LES results. In Fuertes et al.'s study [18], the model was tested on a full-scale wind turbine and the parameter was calibrated based on LiDAR measurements made from the turbine's nacelle. In both studies, the parameters were different and may suggest those parameters vary depending on local conditions.

For wind farm design or operational simulation, it is expensive and time-consuming to calibrate the model with experimental and LES numerical data. Furthermore, using existing parameters from previous numerical and experimental studies may cause inaccurate predictions due to the change of wind turbine specification and local variation. Previous studies have compared several analytical models' prediction with wind turbine operation data [20–22]. In Göçmen et al.'s study [21], several wake models were compared without including the most recent Gaussian-based analytical wake model. In Archer et al.'s study [22], a number of analytical model including two Gaussian-based analytical models, the Bastankhah and Porté-Agel model [13] and the Xie and Archer model [23], were evaluated for the first time against operation data from large wind farms. They concluded six models performed well in three studied wind farms, although the Xie and Archer model and Jensen model had higher prediction accuracy. However, the model's key parameters, wake growth rate, in both Bastankhah and Porté-Agel model [13] and Xie and Archer model [23], were set constant values based on previous LES studies. The field experiment on a full-scale turbine [18] and the LES study at the Horns Rev wind farm [15] suggested that the wake growth rate should not assume to be constant; instead, it is a function of turbulence intensity. Furthermore, in the LES study at the Horns Rev wind farm [15], the assumption of a constant wake growth rate in the Gaussian-based model produced an obvious underestimation of the power output. Allowing for variation in the wake growth rate makes the Bastankhah and Porté-Agel model superior to the Jensen model, which assumes a constant wake growth rate [15].

In order to use the Gaussian-based analytical model operationally, methods avoiding the use of time-consuming and costly experiments and computer simulations for model calibration are needed. Using previous numerical or experimental studies' results may produce inaccurate predictions in different wind farm settings due to the changes in wind turbine specifications. Wind farms are equipped with Supervisory Control And Data Acquisition (SCADA) systems, which record basic meteorological and wind turbine operating conditions, such as wind speed, wind direction, and power generation. The data provides useful information, which has been used extensively in

power prediction, wind turbine health assessment, and operation management [24,25]. Studies have established an understanding of the wake effect in existing wind farms using SCADA data to perform power predictions [20–22,26,27]. The studies that are purely based on SCADA data and data-driven approaches generally can provide an accurate power deficit prediction and inform on wind turbine operation. However, machine learning methods cannot provide a description of the flow field and only gives predictions at locations where turbines are installed. Due to the inability to describe the flow field, machine learning methods cannot be used in wind farm expansion design, wind farm environmental risk assessment, and weather model improvements. A flow physic-based model is still needed. Thoroughly understanding the flow field within the wind farm aids in future engineering decisions and applications.

To improve analytical wake model accuracy for wind power plant simulation, the model must be calibrated based on the specific wind farm setting. Computer simulation and experiments are complex, expensive, and time-consuming, which is not feasible in industrial wind farm applications. In this study, our goal is to develop a simple procedure for calibrating the Gaussian-based analytical wake model to a specific wind farm using SCADA data assimilation. The proposed procedure utilizes a Gaussian-based analytical wake model with SCADA data to describe the flow field within the wind farm and power losses. A comparison between standard wake modeling and proposed wake modeling will be provided. This is the first demonstration of using SCADA data to calibrate the Gaussian-based analytical wake model without using extensive simulation and experiment.

The paper is as follows. In Section 2 the analytical wake models used in this study are described. The wind farm wake modeling procedure with the Gaussian-based analytical model using SCADA data assimilation is proposed in Section 3 and a case study at a large wind farm in Iowa, U.S. is shown. The results and discussion about the case study are included in Section 4, and conclusion and recommendations are provided in Section 5.

2. Description of Models Used for Wind Farm Wake Modeling

In this study, the self-similar Gaussian-based wake model was used to compare with the Jensen model. Similar to the previous study done by Niayifar and Porté-Agel [15], the Gaussian wake model was used to calculate the velocity deficit in the wake region, along with application of a model for representing the effect of cumulative wake effects. The details of the models and their implementation for modeling wind farm follows.

2.1. Jensen Aanalytical Wake Model

The Jensen model assumed a top-hat shape distribution in the wake region [9,10]. The model for the normalized velocity deficit is defined as

$$\frac{\Delta U}{U_\infty} = \frac{U_\infty - U_w}{U_\infty} = \frac{1 - \sqrt{1 - C_T}}{\left(1 + \frac{2k_w x}{d_0}\right)^2}, \tag{1}$$

where U_∞ is the undisturbed ambient velocity, U_w is the wake velocity, C_T is the thrust coefficient, k_w is the wake expansion coefficient, d_0 is the diameter of the wind turbine, and x is the distance downstream of the turbine [9,10].

2.2. Gaussian-Based Analytical Wake Model

Several experimental and numerical studies have suggested the analytical model developed by Bastankhah and Porté-Agel is capable of accurately describing an individual turbine wake [15,18].

The model applies both mass and momentum conservation [13]. The Gaussian shape velocity deficit is represented as

$$\frac{\Delta U}{U_\infty} = \left(1 - \sqrt{1 - \left(\frac{C_T}{8\left(\frac{\sigma}{d_0}\right)^2}\right)}\right) exp\left(-\frac{1}{2\left(\frac{\sigma}{d_0}\right)^2}\left[\left(\frac{z - z_h}{d_0}\right)^2 + \left(\frac{y}{d_0}\right)^2\right]\right), \tag{2}$$

where x, y, and z are the streamwise, spanwise, and vertical coordinates, respectively, and z_h is the turbine hub height [13]. This new approach depends on the thrust coefficient, the wake growth rate, and the wake width at the rotor plane. The model assumes a linear wake expansion [13], similar to the Jensen model. The wake expansion [13] can be written as

$$\frac{\sigma}{d_0} = k^* \frac{x}{d_0} + \epsilon, \tag{3}$$

where k^* is the growth rate and ϵ is the wake width at the rotor plane can be expressed as

$$\epsilon = 0.2\sqrt{\beta}, \tag{4}$$

where β is a function of the thrust coefficient,

$$\beta = \frac{1}{2}\frac{1 + \sqrt{1 - C_T}}{\sqrt{1 - C_T}}. \tag{5}$$

The first Gaussian-based wake model developed by Bastankhah and Porté-Agel assumed the same wake growth rate for both vertical and lateral directions. Later studies have shown that the wake width is not axis-symmetric due to the ground or thermal stratification [23,28]. Xie and Archer proposed a new form of Gaussian-based wake model in which wake width also varies in the y and z directions [23]. Since not all the wind farms are equipped with a meteorology tower, sometimes only limited hub height measurements are available, making calibration in the z direction challenging without using an experimental or numerical study. Therefore, the original form of the Gaussian-based wake model developed by Bastankhah and Porté-Agel is used in this study, described in Equation (2).

For each turbine, the model considers a self-similar Gaussian distribution for the averaged velocity deficit in the wake region, as described in Equations (2)–(5). Unlike the Jensen model, both mass and momentum are conserved in this analytical model. The analytical wake model requires the thrust coefficient, hub height, rotor diameter, and wake growth rate. The thrust coefficient parameter varies as the wind turbine operating condition changes due to the pitch control. In a full-scale commercial turbine, there is a range of wind speeds in which the thrust coefficient holds constant. In this study, we only considered a range of the wind speed in which the thrust coefficient is constant (see Section 3.1. for case study). The wake expansion rate is shown in Equation (3) and the key parameters that need to be determined are k^* and ϵ.

Previous studies based on both the LES [15] and LiDAR experiments [18] have shown the wake growth rate is a linear function of turbulence intensity (TI),

$$k^* = aTI + b, \tag{6}$$

where TI is the incoming streamwise turbulence intensity, and a and b are coefficients to be determined based on regression. Equations (7)–(9) represent the range of previous linear fit results from LES study [15], the LiDAR experiment (a) [18], and the LiDAR experiment (b) [29], respectively,

$$k^* = 0.38TI + 0.004, \tag{7}$$

$$k^* = 0.35TI, \tag{8}$$

$$k^* = 0.3TI. \tag{9}$$

In the analytical wake model, another important parameter is the width of the wake, ϵ, represents the wake at the rotor plane [13]. Bastankhah and Porté-Agel suggested the wake growth rate is a function of the thrust coefficient, expressed in Equations (4) and (5) From fitting the field experiment results, Fuertes et al. [18] suggested ϵ is a function of k^* and can be determined from LiDAR measurement on a full scale wind turbine, shown as

$$\epsilon = -1.91\mathrm{k}^* + 0.34. \tag{10}$$

In this study, we considered Equation (10) in model calibration and velocity deficit prediction.

2.3. Wake Superposition Model

Wind farm modeling relies on understanding the interactions among turbine wakes. A wind turbine within a wind farm may experience the effect of multiple wakes generated from upstream turbines. In the implementation of the analytical wake model, one must consider the cumulative wake effects and wake interactions within the wind farm. Wake superposition models are used to analyze the cumulative wind turbine wake effects, especially where a significant amount of wake overlap each other. Several wind turbine wake superposition models have been proposed. Lissaman proposed a linear superposition of velocity deficit [30]. The linear superposition model is defined as

$$u_i = u_\infty - \sum\nolimits_k (u_\infty - u_{ki}), \tag{11}$$

where u_∞ is ambient inflow condition, u_i is the velocity at turbine i, and u_{ki} is the wake velocity of the turbine k at turbine i. The velocity at turbine i only considers upstream wakes that have influence. The Lissaman model assumed each turbine experienced similar conditions, such as ambient incoming wind speed. In Niayifar and Porté-Agel's study [15], a new wake superposition model adapted ideas from the Lissaman linear superposition model. Instead, the superposition is calculated using the inflow velocity at the turbine, defined as

$$u_i = u_\infty - \sum\nolimits_k (u_k - u_{ki}). \tag{12}$$

Theoretically, linear superposition can result in a negative velocity when multiple wakes closely overlap, making the flow field unrealistic. Katic et al. proposed another approach, which assumed the loss of kinetic energy from wake interaction can be presented by the sum of the energy deficit of each wake [10], the model defined as

$$u_i = u_\infty - \sqrt{\sum\nolimits_k (u_\infty - u_{ki})^2}. \tag{13}$$

Unlike Lissaman's approach, the approach proposed by Katic et al. has a square root function that ensures the velocity remains positive. Vogel and Willden evaluated different superposition models based on CFD results and found the performances vary based on the wind farm layout when turbines operate at below rated wind speed [31]. For the sake of simplicity, in this study we used linear superposition and considered only the incoming wind speed as in Equation (12).

2.4. Wake Model Calibration

The key parameter in Bastankhah and Porté-Agel model is the wake growth rate k^*. In the Archer et al. study, the wake growth rate was set to a constant value [22], which demonstrated inaccuracies in wind farm modeling [15,18]. Based on previous LES [15] and field [18] studies' suggestions, the wake growth rate is assumed to be a function of turbulence intensity. Multiple point velocity measurements are needed to estimate the exponential function because the Equation 2 is an exponential function. Due

to the lack of multiple points of measurements in the wake, in this study only the maximum velocity deficit at the center of wake where $y = 0$ and $z = z_h$ is considered, and Equation 2 becomes

$$\frac{\Delta U}{U_\infty} = 1 - \sqrt{1 - \frac{C_T}{8\left(k^* \frac{x}{d} + \varepsilon\right)^2}}. \tag{14}$$

Rearranging Equation (14) and solving for k^*, where $\varepsilon = -1.91k^* + 0.34$ [18] yields,

$$k^* = \frac{\left[\sqrt{-\frac{C_T}{8\left(-2\frac{\Delta U}{U_\infty} + \left(\frac{\Delta U}{U_\infty}\right)^2\right)}} - 0.34\right]}{\frac{x}{d} - 1.91}. \tag{15}$$

In Equation (15), the velocity deficit can be determined based on the wind speed data from SCADA and the GPS coordinate of the wind turbine. The thrust coefficient C_T is assumed to be constant within a range of wind speeds, which is typical for most of the utility-scale turbines. In this study, the C_T is set to 0.82 at the 5 – 10 m/s wind speed range, with details outlined in Section 3.1.

Therefore, only the maximum velocity deficit is needed and can be determined based on wind speed data at a specific wind direction when the downstream turbine is at the center of the upstream turbine's wake, shown in Figure 1. The specific wind direction is determined using the GPS coordinates of the two turbines.

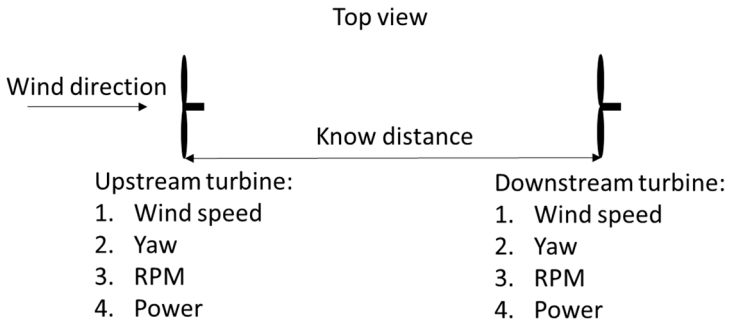


Figure 1. Annotated schematic of a pair of turbines.

In the model calibration process, 10 minutes average SCADA data were used. For each case, wind speed and yaw direction were used to calculate the maximum velocity deficit and ensured the downstream turbine was at the center of the wake generated by the upstream turbine. Other data, such as RPM and power, were used to ensure that cases are selected when both turbines function as expected based on the manufacturer's specifications. A total of 52 cases where data quality has been ensured at 11 different distances were selected for model calibration. The SCADA data of velocity deficit based on the pairs of turbines are shown in Figure 2.

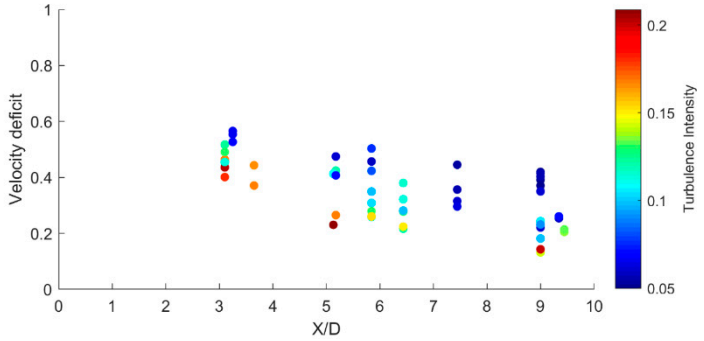


Figure 2. Supervisory Control And Data Acquisition (SCADA) data of velocity deficit based on paired turbines.

Figure 2 shows the velocity deficit decreased as the distance between turbines increased. After obtaining the velocity deficit from each pair turbine case, substituting the velocity deficit into Equation (15) allows for the solving of the wake growth rate k^*. Similar to previous research, we determined the relationship between k^* and upstream turbine's longitudinal turbulence intensity, which was measured by nacelle anemometers.

The relationship between wake growth rate and longitudinal turbulence intensity is shown in Figure 3, the general trend is similar to previous studies [15,18]. By comparing with LES and full-scale LiDAR measurements, using the maximum velocity deficit at the center of the wake can also produce similar results and demonstrate the analytical model's calibration. Similar to the previous study, the wake growth rate increased as the longitudinal turbulence intensity increased, which means the wake recovered faster as the turbulence intensity increased. Figure 3 also suggests that the wake growth rate might not only depend on the turbulence intensity but also other variables. In the study by Iungo [32] he suggests that different thermal stability has impacts on the wake recovery. Other studies have also suggested that wind veer [29] and vertical velocity component fluctuations [33] play important role in wake structure. Future study is needed to account for thermal stability, wind veer, and vertical velocity component in the simple analytical wake model.

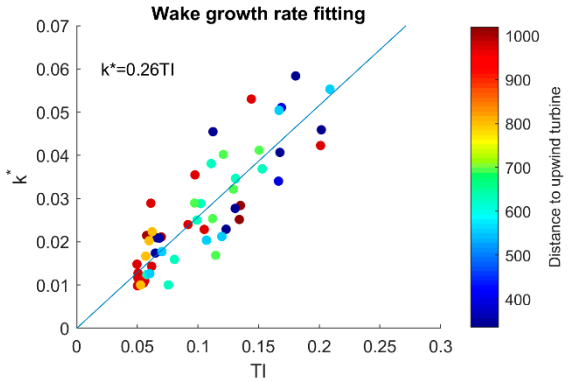


Figure 3. Relationship between the wake growth rate and longitudinal turbulence intensity. Data were selected from 52 cases at 11 different distances. The line is the linear fit of the data, $R^2 = 0.73$.

3. Wind Farm Wake Modeling Procedure

In this study, a procedure to model the wind farm wake effect using the Gaussian-based analytical wake model was proposed. The modeling can be done without using extensive computation and has the practicality needed for commercial purposes. In this section, we demonstrated the proposed procedure for wind farm wake modeling and a case study at a large commercial wind farm in Iowa, USA.

3.1. Wind Farm Description

The study wind farm located in central Iowa has 51 Siemens 2.3 MW turbines. The turbines have an 80 m hub height and a 108 m diameter rotor. The terrain around and within the wind farm is generally flat. The maximum elevation difference between turbines does not exceed 20 m (1/5 of rotor diameter) and average elevation difference between turbines is less than 10 m. The wind farm map and layout are shown in Figure 4.

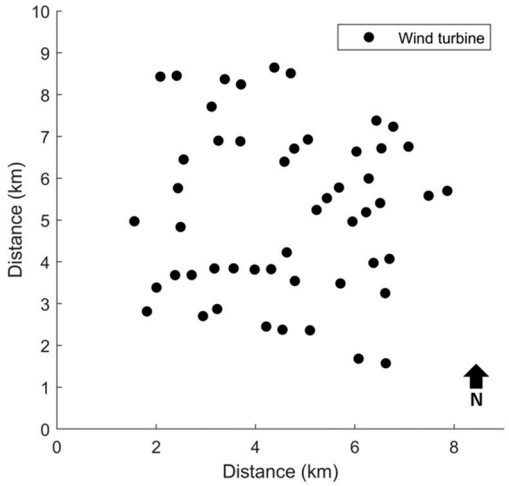


Figure 4. Case study wind farm layout.

As shown in Figure 4, the study wind farm had an irregular spacing. The wind turbines had a cut-in wind speed of 3 m/s. The power coefficient of the turbine and the blade pitch angle as a function of incoming wind speed is shown in Figure 5.

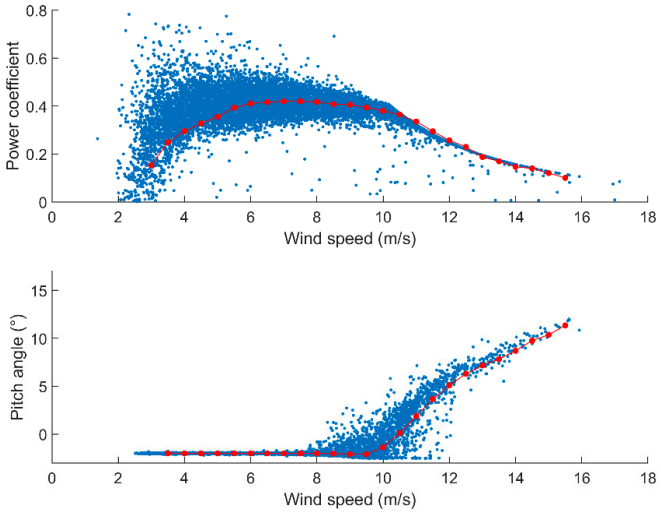


Figure 5. Power coefficient and blade pitch angle as a function of the wind speed for the study turbines from SCADA data. The 10 minutes average values are shown in blue dots and binned averages are red.

As shown in Figure 5, the power coefficient was constant and close to 0.41 at wind speeds between 5 and 10 m/s. The value of the power coefficient was determined by using the average value of the data from 5 to 10 m/s and bins of 0.5 m/s. At this range of wind speeds, turbines operate optimally and normally. When the wind speed was above 10 m/s, the pitch control systems started to reduce the efficiency of the blades so that it reduced the thrust coefficient. In this case study, a constant $C_T = 0.82$ was assumed for 5–10 m/s wind speed range.

3.2. SCADA Data Pre-Processing

All the turbines within the wind farm were equipped with the SCADA system. The SCADA data contains the following information: sitewide wind direction (°), sitewide wind speed (m/s), power generation (kW), ambient temperature at hub height (°C), blades pitch angle (°), rotor RPM, wind speed (m/s), yaw direction respect to the north (°), and wind turbine error codes. Wind speed and power generation were also recorded.

Before the wake modeling process, the SCADA data was selected based on the wind farm operational conditions. As described in Section 3.1, only the cases within 5–10 m/s range of wind speed were used. For this study wind farm, we assumed a flat terrain and a uniform inflow condition for all wind directions. The sitewide wind direction and averaged yaw direction for each turbine were compared. When the difference between sitewide wind direction and averaged yaw direction is less than 2°, the sitewide wind direction was used to represent the uniform wind direction. The front row turbine was determined by the uniform wind direction. The uniform incoming wind speed was determined by averaging the front row turbines' wind speed measurement from SCADA. When a turbine experienced wake effects, and the wind speed was below the cut-in wind speed, the turbine was assumed not to contribute to the wake effect on the downstream turbines.

3.3. Model Implementation

In this case study, the implementation of the analytical models was done using MATLAB, but one can use the same algorithm in different programming languages. The calculation domain is a matrix that represents a 10 km by 10 km square with a grid size of 1 m. Each grid in the calculation domain was filled in with a percentage of velocity remain (PVR). The initial value of PVR was set to 1, and the PVR is defined as

$$percentage\ of\ velocity\ remain = 1 - \frac{U_\infty - U_w}{U_\infty}. \tag{16}$$

Turbines are placed in the domain based on their GPS coordinates. After the computational domain was set up and turbine specifications defined, a rotation matrix rotated the wind farm map to ensure the flow in the computational domain comes from the left to right (along the x-axis). The rotation matrix is defined as

$$R = \begin{bmatrix} \cos(\theta) & \sin(\theta) \\ -\sin(\theta) & \cos(\theta) \end{bmatrix}. \tag{17}$$

Afterward, the rotation matrix can also be used to rotate the wind farm map with respected to north.

After the wind farm map is rotated based on the wind direction, the order of the turbines is determined by using each turbine's x-coordinate. The order of the turbine used for a wake calculation order ensures the upstream turbine's wake was calculated first. For each turbine, the incoming wind condition was determined by using the averaged value from previous grid points respective to the rotor plane. Since the existing analytical turbulence intensity models [34,35] cannot accurately predict turbulence intensity for a large wind farm with irregular spacing, the turbulence intensity data were taken directly from SCADA.

The velocity deficit for each turbine in the order from upwind was calculated by using the calibrated analytical wake model, described in Section 2.4. After determining each turbine's wake velocity deficit, the grid point values behind the rotor plane were updated based on the linear superposition (method described in Section 2.3). Following the completion of the calculation, a PVR matrix was outputted, providing the velocity deficit within the domain. Finally, the prediction of the wind speed can be obtained by multiplying the PVR matrix with the incoming wind speed matrix, shown in Figure 6.

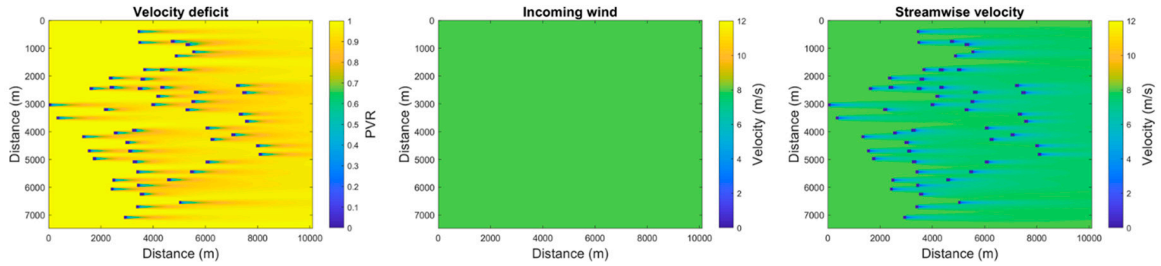


Figure 6. Generation of streamwise velocity map based on velocity deficit map multiplied from the average incoming velocity.

3.4. Power Prediction

The streamwise velocity prediction derived from the wake model is directly used for power prediction. The industrial standard power prediction method uses wind speed and the manufacturer's power curve. The empirical power curve of the turbines in the study is shown in Figure 7. In addition to wind speed and power data from 261,082 data points across the entire wind farm, the turbulence intensity measured at hub height is also shown. The color scale of the turbulence intensity in Figure 7 suggests that the turbulence intensity also has an impact on the power prediction and also support by previous studies [36,37]. High turbulence intensity tended to lay above the power curve, suggesting that the turbine outperformed the standard operating condition under those conditions. Low turbulence intensity tended to lay below the power curve, indicating that the turbines tended to underperform compared to the standard operating condition in those circumstances.

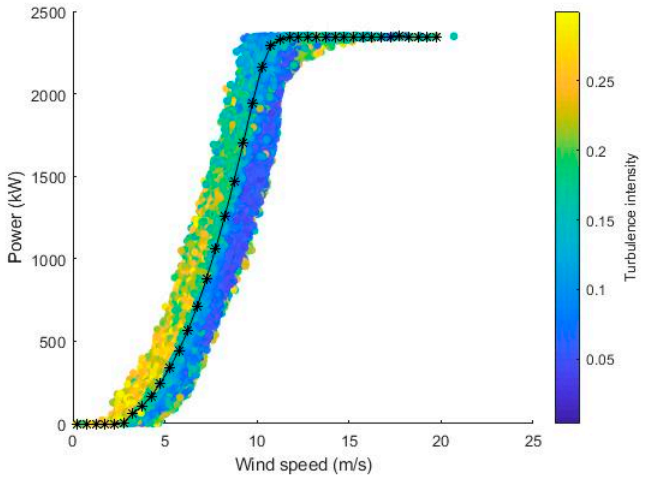


Figure 7. Power curve for the study turbine, derived using ten-minute SCADA data from 1 July to 15 October 2018. The 10 minutes values are shown in dots, and the color scale represents 10 minutes average turbulence intensity measurement on top of the nacelle. The binned averages are in black.

In a large-scale wind farm, different turbine will experience different turbulence intensity. The wind turbine located in the inner portion of the wind farm will likely experience higher turbulence intensity than the turbines located closer to the edge. Vahidzadeh and Markfort's study suggest that incorporating turbulence intensity for power prediction would reduce the prediction error [38]. Thus, to accurately predict the wind turbine power generation, a power surface with turbulence intensity, wind speed, and power were used in this study, shown in Figure 8. After the implementation of the power surface, the power prediction accuracy increases compared with the standard empirical power curve. The improvement of the performance is shown in Figure 9

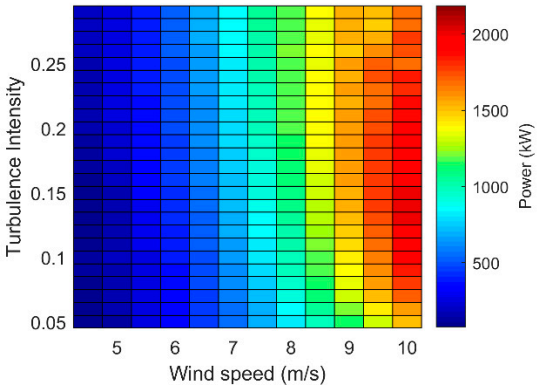


Figure 8. Power surface relating turbine power to wind speed and turbulence intensity.

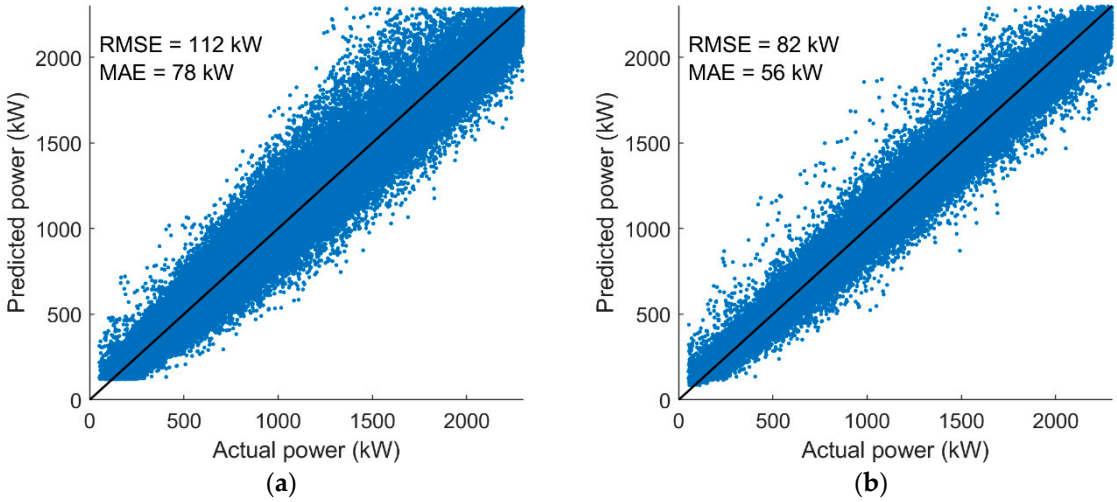


Figure 9. Performance of the standard power curve and power surface based on turbulence intensity and wind speed. (**a**) Standard power curve and (**b**) modified power surface.

4. Case Study Results and Discussions

This section presented a case study demonstrating the proposed procedure for Gaussian-based analytical wake modeling with wind turbine SCADA data. The proposed procedure introduced in Section 3 and its results were compared with the industry standard model, the Jensen model [9,10]. Since the study wind farm is an onshore wind farm and the surrounding land is mostly agricultural, a value of 0.075 was selected for the wake effect decay constant in the Jensen model. The time-window for this case study was 10 minutes.

To validate the model's ability to analyze individual turbine wakes, an array of three turbines were selected from the study wind farm. Since the wind farm is irregularly spaced and prevailing wind directions are southeast and northwest, only an array of three turbines were available for the array of the wakes interaction demonstration. These three turbines are in the northeast corner of the wind farm with 630 m (6 rotor diameters) between the first and second turbines, and 690 m (6 rotor diameters) between the second and the third turbine, shown in Figure 10. Figure 11 shows the normalized power output generated from the proposed procedure and the Jensen model for the three-turbine-array under perfect alignment at the center of wake (a) and partial wake condition with 3° degree wind direction offset (b). The prediction of the power was calculated under a carefully selected 10 minutes average case. The wind direction and wind speed were constant for a period of time preceding the analyzed 10 minute time window to avoid the turbine's response time affecting the results. The turbulence intensity was selected based on the suggestion from Fuertes et al.'s study [18] to avoid the near-wake region, where the velocity deficit is not well represented by the Gaussian-based analytical model.

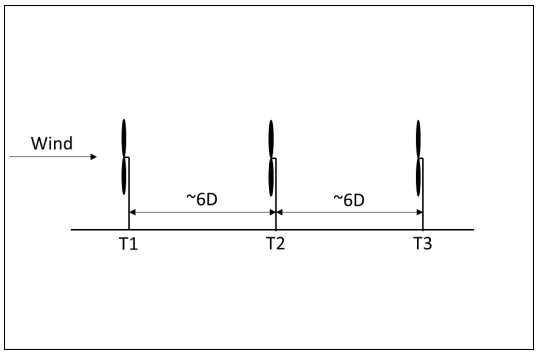


Figure 10. Layout of the three turbines array.

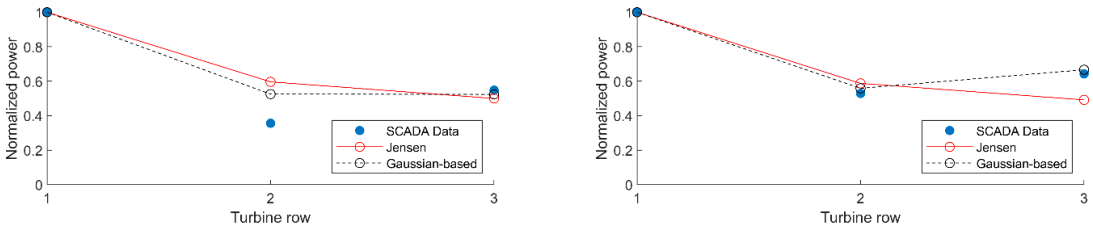


Figure 11. Comparison of simulated and observed power output under perfect alignment at the center of the wake with a wind direction of 158° (**a**) and partially waked condition with a wind direction of 155° (**b**).

Both models tended to produce errors in the power prediction of the second turbine, but the Gaussian-based wake model outperformed the Jensen model in overall accuracy. As shown in Figure 11, the Jensen model tended to underestimate the power output of the third turbine, which was also observed in the Horns Rev wind farm study [15]. Under partial wake conditions, the Gaussian-based analytical wake model had better accuracy in predicting the power output because the Gaussian-based wake model can realistically predict the maximum velocity deficit, shown in previous studies [13,15,18]. As shown in Figure 12, the Jensen model produces an unrealistic velocity deficit in the wake, which has a uniform velocity distribution in the spanwise direction. This means the Jensen model underestimates the velocity deficit in the far wake region. The Gaussian-like velocity deficit assumption enables the model to accurately predict a more realistic maximum velocity deficit under partial wake condition. The wake growth rate parameter and turbulence intensity are adjusted according to the local streamwise turbulence intensity, so the wake recovery prediction is also more accurate than the Jensen model.

To demonstrate the performance of the Gaussian-based analytical wake model for a wind farm, we conducted a sitewide average wind speed and sitewide total power prediction assessment by using three different methods: a SCADA calibrated Gaussian-based model with a variable wake growth rate k^*, the standard Jensen model, and a Gaussian-based model with constant k^*. In this case study, ten-minutes averaged SCADA was used, and all turbines within the wind farm were considered. The sitewide average wind speed prediction assessment is done by comparing three models' prediction of the average wind speed across all the operating turbines. The sitewide total power prediction assessment is done by comparing three models' prediction of the total power of the wind farm generation. To assess the three models' performance, Mean Absolute Percentage Error (MAPE), Root Mean Square Error (RMSE), and Mean Squared Error (MSE) were reported.

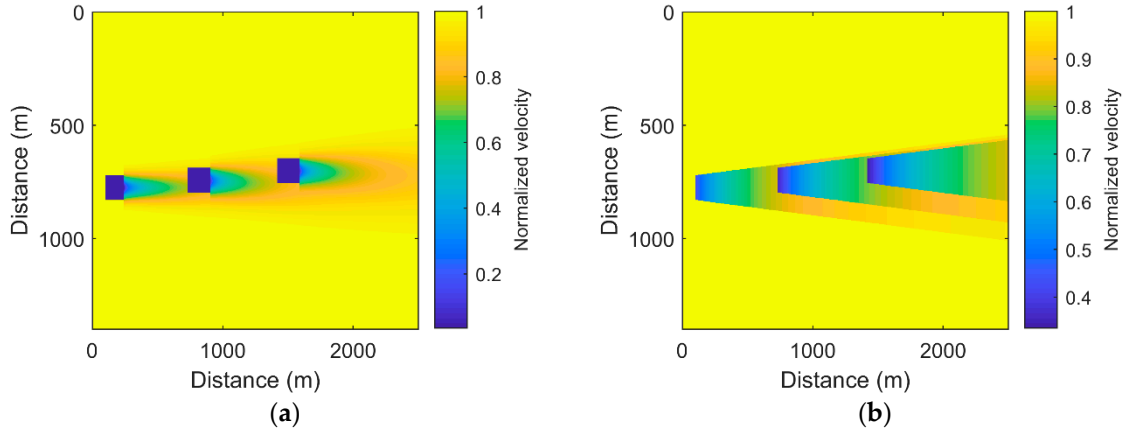


Figure 12. Streamwise wake of the three turbine array under the partial wake condition: (**a**) Gaussian-based analytical wake model and (**b**) Jensen model.

The cases were selected from a period of 4 months. A consistent data selection process was implemented. The chosen cases had stationary wind speed and wind direction for over a half-hour period. In this period, the wind speed for each operating turbine had to remain in the wind speed range of 5 – 10 m/s with at least 49 of the 51 turbines in the study wind farm operating. Situations where nearby patches of trees made determining the incoming wind speed too hard to determine were discarded. Overall, 100 cases were selected from a period of 4 months. Figure 13 shows the percent relative error of the sitewide total power prediction for three models. Table 1 shows models' prediction errors of the selected 100 cases. In the comparison, a constant wake growth rate, $k^* = 0.03$ were used, which is the same as the previous study [22]. The Gaussian-based analytical wake model with constant k^* has similar performance with the Jensen model, but the Jensen model performed slightly better. After calibrating the Gaussian-based analytical model with SCADA data using the proposed procedure, the Gaussian-based analytical model is found to outperform the Jensen model and produced less error for predicted wind farm total power. A variable wake growth rate for each turbine significantly improves the prediction. The variable wake growth rate can simulate a more realistic wind farm condition, where the wake recovers faster further away from the front row of the wind farm due to a higher turbulence intensity compared to ambient conditions. Increasing the number of cases did not significantly impact the results.

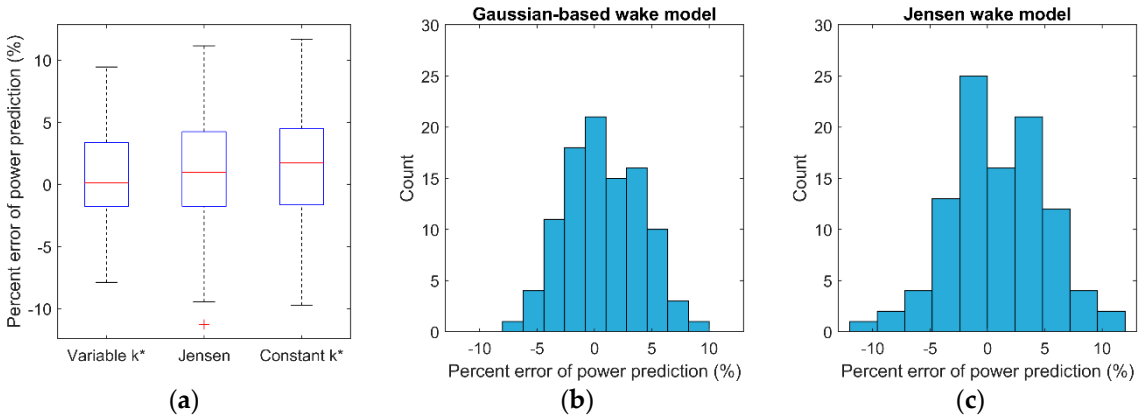


Figure 13. Comparison of sitewide total power prediction from 100 selected cases: (**a**) boxplot of percent error of power prediction using three different methods; (**b**) histogram of percent error of power prediction using the Gaussian-based model with variable k^*; and (**c**) histogram of percent error of power prediction using the Jensen model.

Table 1. Models' sitewide total power prediction errors in 100 selected cases.

Error Terms	Gaussian-Based Model with Variable k^*	Jensen Model	Gaussian-Based Model with Constant k^*
MAPE	2.77%	3.54%	3.67%
RMSE	1579 kW	2012 kW	2091 kW
MSE	2.5 GW	4.0 GW	4.4 GW

Furthermore, in sitewide average wind speed prediction, the Gaussian-based model with variable k* outperformed the Jensen model and Gaussian-based model with constant k^*. Figure 14 shows the percentage relative error of the sitewide averaged wind speed prediction for 100 selected cases, and Table 2 shows the models' prediction errors of the 100 selected cases. The sitewide averaged wind speed was obtained by averaging all the wind speed at each turbine. In most cases, the sitewide averaged wind speed was less than uniform incoming wind speed. In terms of sitewide average wind speed prediction, the Gaussian-based model with variable k^* had less error, according to Table 2. The Jensen model tended to overestimate the velocity deficit because of the assumption of a top-hat shape velocity deficit profile, which overestimated in the far-wake region.

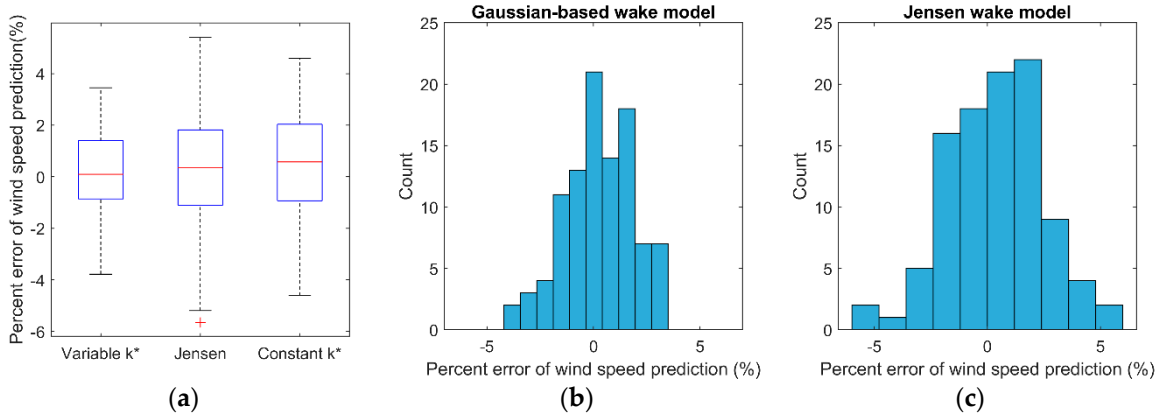


Figure 14. Comparison of sitewide average wind speed prediction from 100 selected cases: (**a**) boxplot of the percent error of sitewide average wind speed prediction using three different methods; (**b**) histogram of the percent error of sitewide average wind speed prediction using the Gaussian-based model with variable k^*; and (**c**) histogram of the percent error of sitewide average wind speed prediction using the Jensen model.

Table 2. Models' sitewide averaged wind speed prediction errors in 100 selected cases.

Error Terms	Gaussian-Based Model with Variable k^*	Jensen Model	Gaussian-Based Model with Constant k^*
MAPE	1.31%	1.70%	1.73%
RMSE	0.12 m/s	0.15 m/s	0.15 m/s
MSE	0.014 m/s	0.024 m/s	0.023 m/s

In the following, the models' predictions of individual turbines will be discussed. The study wind farm is located in central Iowa, USA. As shown in Figure 15, the main direction of the wind was northwest and southeast. The average wind speed near the ground was approximately 10.4 mph (4.6 m/s).

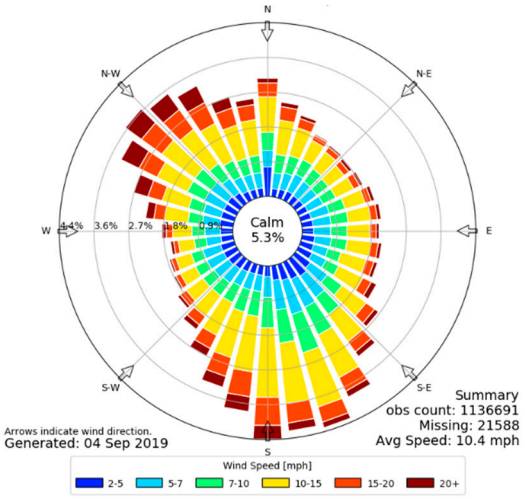


Figure 15. Wind rose measured at an airport for 25 years, about 14 miles SW of the wind farm. Data obtained from Iowa State University, Iowa Environmental Mesonet [39]. The length of the bars indicates the frequency in percentage units.

Two cases that represent the main wind directions, 186° and 307° were selected. The flow field prediction of the calibrated Gaussian-based analytical wake model and mean average percentage error (MAPE) of wind speed prediction for all turbines is shown in Figure 16. Figure 16a shows the flow field of the 186° wind direction and Figure 16b shows the flow field of the 307° direction. In both directions, by comparing predictions and true values, many errors can be observed in a certain region of the wind farm. Errors occurred at the front row turbine and the turbine in the far end region due to the uniform wind flow assumption. In addition, the Gaussian-based wake model is very sensitive to the wind direction due to the assumption of Gaussian shape, especially in the far-wake region. Assuming a uniform wind direction can result in inaccurate predictions of the velocity deficit because the model does not account for wind direction variation. This has observed for some areas of the wind farm. However, when the condition was ideal and ambient condition was stationary for some time, the prediction accuracy increased. The Gaussian-based wake model can accurately predict the power and velocity deficit of the downstream turbines.

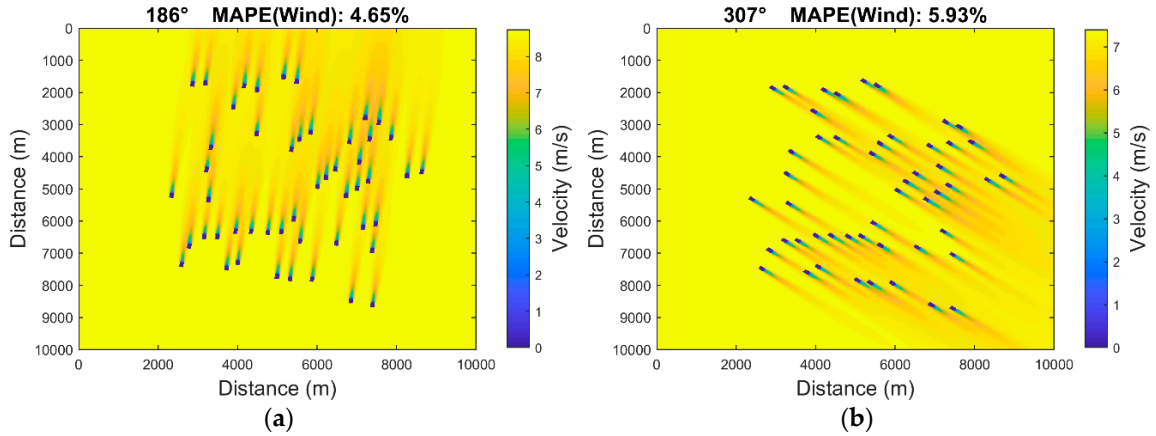


Figure 16. Gaussian-based analytical wake model flow field prediction for wind direction: (**a**) 186° and (**b**) 307°.

In general, when predicting the individual turbine's wind speed and power generation, the calibrated Gaussian-based model exhibits higher accuracy than the Jensen model, shown in Table 3. The Gaussian-based model has a lower mean average percentage error (MAPE) and mean square error (MSE) for both wind speed and power prediction of individual turbines within the wind

farm. The range of the percent error in power and wind speed prediction for individual turbines in each case study are shown in Table 4. In comparison with Jensen model, the Gaussian-based model has a smaller range of percent error in both power and wind speed prediction.

Table 3. 10 minutes average case study prediction errors.

Error Terms	Gaussian-Based Model	Jensen Model	Gaussian-Based Model	Jensen Model
	Case Study at 186°		Case Study at 307°	
MAPE (Wind)	4.65%	4.83%	5.93%	6.42%
MAPE (Power)	11.7%	13.0%	16.0%	17.3%
MSE (Wind)	0.23 m/s	0.27 m/s	0.28 m/s	0.35 m/s
MSE (Power)	37 MW	43 MW	37 MW	47 MW

Table 4. Range of percent error in power and wind speed prediction for individual turbine within the wind farm.

Case Study at Wind Direction	Range of Percent Error in Power Prediction		Range of Percent Error in Wind Speed Prediction	
	186°	307°	186°	307°
Gaussian-based model	[−32%, 56%]	[−37%, 70%]	[−11%, 20%]	[−15%, 25%]
Jensen model	[−44%, 58%]	[−53%, 87%]	[−16%, 20%]	[−22%, 29%]

Even though the accuracy of the individual turbine may vary according to the wind direction and other atmospheric conditions because of the complexity in nature, the model is still able to provide a reasonable prediction for sitewide average wind speed and total power generation. Figure 17 shows a timeseries of sitewide average wind speed and sitewide average yaw direction from SCADA data as well as prediction errors from the Gaussian-based analytical wake model. The errors were the largest when the wind speed and yaw direction were not stationary. As the wind speed and yaw direction remained constant for a period of time, both wind speed and power prediction errors reduced. Figure 17 provides evidence that the proposed procedure, and the Gaussian-based wake analytical model has the potential to accurately model the wind farm wake effects and power prediction for real-time operation of a wind farm.

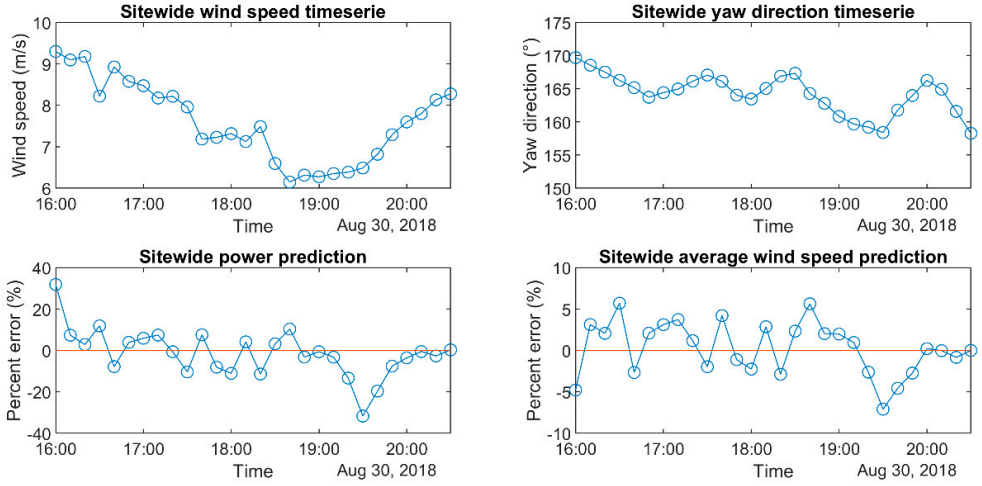


Figure 17. Timeseries of sitewide SCADA data and model prediction errors. The red line is the zero reference line.

Future improvement is needed to reduce the error in the period when the inflow conditions are evolving. Considering wind/wake transport time across the wind farm and variation in wind direction for different regions would improve the model's accuracy in real-time modeling. Assuming a uniform incoming wind speed is a simple approach but not realistic in all wind farm conditions. Taking a wind speed gradient across the wind farm into account can provide more realistic modeling results. In addition, turbine yaw misalignment and turbine control should also be considered. Misalignment in the yaw direction is inevitable in the real wind farm operation. The yaw error can cause wake deflection, so a simple wake model may not accurately represent the behavior of wakes. Future analysis should consider wind farm yaw error and incorporate a wake deflection model.

The proposed procedure for calibration of the Gaussian-based analytical wake model for wind farm modeling provides a simple approach for wind farm operation analysis using only SCADA data. The proposed procedure enables the Gaussian-based wake model to simulate streamwise velocity on a horizontal plane at the hub height level using real-time data. The Gaussian-based wake model can model sitewide power generation and average wind speed, and it can provide insight into the power deficit at varied wind direction. With the proposed procedure for calibration of the model, the model has the potential to perform a real-time analysis of the wind turbine wake effects in a wind farm, identify waked regions, and determine turbines, which may be shut-off due to low wind speed. Incorporating turbulence intensity, the Gaussian-based model has the potential to model power based on specific operating conditions.

Understanding the wake behavior within the wind farm is very important for future applications. The wake model can help biologists to determine low wind speed regions within and near wind farms for wildlife impact mitigation. The model can also help to improve weather models, such as Weather Research and Forecasting Model (WRF), to account for wind farm wake effects in real-time.

5. Conclusions and Recommendations

A procedure for calibration of the Gaussian-based analytical wake model using operational wind turbine SCADA data was proposed. The procedure incorporated the Gaussian-based analytical wake model developed by Bastankhah and Porté-Agel [13] and a wake superposition model. This is the first time an analytical wake model was calibrated based on wind turbine operational data. To simulate more realistic flow conditions, the wake growth rate is a variable that is allowed to change according to local turbulence intensity. The wake modeling process can provide a description of the time-average flow field of the wind farm. The power is predicted using the newly proposed modified power surface including local turbulence intensity.

A case study at a large onshore irregularly spacing wind farm demonstrated the proposed procedure. The Gaussian-based analytical wake model was calibrated using SCADA data from wind turbine pairs across the wind farm. After calibration, the model was compared with the standard Jensen model and Gaussian-based model with constant wake growth rate. The results show that the proposed procedure and Gaussian-based analytical wake model shows an approximate 1% improvement in sitewide power prediction compared to the Jensen model and the Gaussian-based wake model with constant wake growth rate. The results have shown that after calibrating the Gaussian-based wake model using the SCADA data, the prediction accuracy was better than the model, which utilized a calibrated coefficient from previous studies. We also demonstrated that the Gaussian-based model had the potential to model the wake dynamics within the wind farm in real-time. The comparison between model and SCADA data demonstrated that the model had the ability to provide information about the flow field within and around the wind farm. The proposed procedure for the Gaussian-based analytical wake model provides a simple method for the wind farm operator to calibrate a wake model specifically for an existing wind farm, without conducting expensive experiments or computational flow simulations.

Future research should focus on the use of simple analytical approach in evolving flow conditions and incorporate change in incoming wind speed and variation of wind direction across the wind farm. Future analysis should also consider wake deflection model and yaw misalignment.

Author Contributions: This study was done as a part of J.T. master's studies supervised by C.D.M. All authors have read and agreed to the published version of the manuscript.

Funding: This research was funded by MidAmerican Energy Company.

Acknowledgments: The authors would like to acknowledge MidAmerican Energy Company for support in providing wind farm operations data.

Conflicts of Interest: The authors declare no conflict of interest.

References

1. Wind Energy in the United States. Available online: https://www.awea.org/wind-101/basics-of-wind-energy/wind-facts-at-a-glance (accessed on 21 February 2020).
2. *Wind Vision: A New Era for Wind Power in the United States*; U.S. Department of Energy: Washington, DC, USA, 2015.
3. Veers, P.; Dykes, K.; Lantz, E.; Barth, S.; Bottasso, C.L.; Carlson, O.; Clifton, A.; Green, J.; Green, P.; Holttinen, H. Grand challenges in the science of wind energy. *Science* **2019**, *366*, eaau2027. [CrossRef]
4. Markfort, C.D.; Zhang, W.; Porté-Agel, F. Turbulent flow and scalar transport through and over aligned and staggered wind farms. *J. Turbul.* **2012**, *13*, N33. [CrossRef]
5. Porté-Agel, F.; Bastankhah, M.; Shamsoddin, S. Wind-turbine and wind-farm flows: A review. *Bound. Layer Meteorol.* **2020**, *174*, 1–59. [CrossRef] [PubMed]
6. Zhang, W.; Markfort, C.D.; Porté-Agel, F. Experimental study of the impact of large-scale wind farms on land–atmosphere exchanges. *Environ. Res. Lett.* **2013**, *8*, 015002. [CrossRef]
7. Markfort, C.D.; Zhang, W.; Porté-Agel, F. Analytical Model for Mean Flow and Fluxes of Momentum and Energy in Very Large Wind Farms. *Bound. Layer Meteorol.* **2018**, *166*, 31–49. [CrossRef]
8. Barthelmie, R.J.; Larsen, G.; Frandsen, S.; Folkerts, L.; Rados, K.; Pryor, S.; Lange, B.; Schepers, G. Comparison of wake model simulations with offshore wind turbine wake profiles measured by sodar. *J. Atmos. Ocean. Technol.* **2006**, *23*, 888–901. [CrossRef]
9. Jensen, N.O. *A note on Wind Generator Interaction*; Risoe National Laboratory: Roskilde, Denmark, 1983.
10. Katic, I.; Højstrup, J.; Jensen, N.O. A simple model for cluster efficiency. In Proceedings of the European Wind Energy Association Conference and Exhibition, Rome, Italy, 7–9 October 1986; pp. 407–410.
11. Larsen, G.C. *A Simple Wake Calculation Procedure*; Risø National Laboratory: Roskilde, Denmark, 1988.
12. Frandsen, S.; Barthelmie, R.; Pryor, S.; Rathmann, O.; Larsen, S.; Højstrup, J.; Thøgersen, M. Analytical modelling of wind speed deficit in large offshore wind farms. *Wind Energy Int. J. Prog. Appl. Wind Power Convers. Technol.* **2006**, *9*, 39–53. [CrossRef]
13. Bastankhah, M.; Porté-Agel, F. A new analytical model for wind-turbine wakes. *Renew. Energy* **2014**, *70*, 116–123. [CrossRef]
14. Gaumond, M.; Réthoré, P.-E.; Bechmann, A.; Ott, S.; Larsen, G.C.; Diaz, A.P.; Hansen, K.S. Benchmarking of wind turbine wake models in large offshore windfarms. In Proceedings of the Science of Making Torque from Wind 2012: 4th Scientific Conference, Oldenburg, Germany, 9–11 October 2012.
15. Niayifar, A.; Porté-Agel, F. Analytical modeling of wind farms: A new approach for power prediction. *Energies* **2016**, *9*, 741. [CrossRef]
16. Chamorro, L.P.; Porté-Agel, F. A wind-tunnel investigation of wind-turbine wakes: Boundary-layer turbulence effects. *Bound. Layer Meteorol.* **2009**, *132*, 129–149. [CrossRef]
17. Wu, Y.-T.; Porté-Agel, F. Large-eddy simulation of wind-turbine wakes: Evaluation of turbine parametrisations. *Bound. Layer Meteorol.* **2011**, *138*, 345–366. [CrossRef]
18. Carbajo Fuertes, F.; Markfort, C.D.; Porté-Agel, F. Wind turbine wake characterization with nacelle-mounted wind lidars for analytical wake model validation. *Remote Sens.* **2018**, *10*, 668. [CrossRef]
19. Hansen, K.S.; Barthelmie, R.J.; Jensen, L.E.; Sommer, A. The impact of turbulence intensity and atmospheric stability on power deficits due to wind turbine wakes at Horns Rev wind farm. *Wind Energy* **2012**, *15*, 183–196. [CrossRef]

20. Barthelmie, R.J.; Hansen, K.; Frandsen, S.T.; Rathmann, O.; Schepers, J.G.; Schlez, W.; Phillips, J.; Rados, K.; Zervos, A.; Politis, E.S.; et al. Modelling and measuring flow and wind turbine wakes in large wind farms offshore. *Wind Energy* **2009**, *12*, 431–444. [CrossRef]
21. Göçmen, T.; Van der Laan, P.; Réthoré, P.-E.; Diaz, A.P.; Larsen, G.C.; Ott, S. Wind turbine wake models developed at the technical university of Denmark: A review. *Renew. Sustain. Energy Rev.* **2016**, *60*, 752–769. [CrossRef]
22. Archer, C.L.; Vasel-Be-Hagh, A.; Yan, C.; Wu, S.; Pan, Y.; Brodie, J.F.; Maguire, A.E. Review and evaluation of wake loss models for wind energy applications. *Appl. Energy* **2018**, *226*, 1187–1207. [CrossRef]
23. Xie, S.; Archer, C. Self-similarity and turbulence characteristics of wind turbine wakes via large-eddy simulation. *Wind Energy* **2015**, *18*, 1815–1838. [CrossRef]
24. Kusiak, A.; Li, W. The prediction and diagnosis of wind turbine faults. *Renew. Energy* **2011**, *36*, 16–23. [CrossRef]
25. Kusiak, A.; Zheng, H.; Song, Z. Models for monitoring wind farm power. *Renew. Energy* **2009**, *34*, 583–590. [CrossRef]
26. Howland, M.F.; Dabiri, J.O. Wind farm modeling with interpretable physics-informed machine learning. *Energies* **2019**, *12*, 2716. [CrossRef]
27. Kusiak, A.; Zheng, H.; Song, Z. Wind farm power prediction: A data-mining approach. *Wind Energy Int. J. Prog. Appl. Wind Power Convers. Technol.* **2009**, *12*, 275–293. [CrossRef]
28. Abkar, M.; Porté-Agel, F. Influence of atmospheric stability on wind-turbine wakes: A large-eddy simulation study. *Phys. Fluids* **2015**, *27*, 035104. [CrossRef]
29. Brugger, P.; Fuertes, F.C.; Vahidzadeh, M.; Markfort, C.D.; Porté-Agel, F. Characterization of Wind Turbine Wakes with Nacelle-Mounted Doppler LiDARs and Model Validation in the Presence of Wind Veer. *Remote Sens.* **2019**, *11*, 2247. [CrossRef]
30. Lissaman, P. Energy effectiveness of arbitrary arrays of wind turbines. *J. Energy* **1979**, *3*, 323–328. [CrossRef]
31. Vogel, C.R.; Willden, R.H.J. Investigation of wind turbine wake superposition models using Reynolds-averaged Navier-Stokes simulations. *Wind Energy* **2020**, *23*, 593–607. [CrossRef]
32. Iungo, G.V. Experimental characterization of wind turbine wakes: Wind tunnel tests and wind LiDAR measurements. *J. Wind Eng. Ind. Aerodyn.* **2016**, *149*, 35–39. [CrossRef]
33. Larsen, G.C.; Madsen, H.A.; Thomsen, K.; Larsen, T.J. Wake meandering: A pragmatic approach. *Wind Energy Int. J. Prog. Appl. Wind Power Convers. Technol.* **2008**, *11*, 377–395. [CrossRef]
34. Crespo, A.; Herna, J. Turbulence characteristics in wind-turbine wakes. *J. Wind Eng. Ind. Aerodyn.* **1996**, *61*, 71–85. [CrossRef]
35. Ishihara, T.; Qian, G.-W. A new Gaussian-based analytical wake model for wind turbines considering ambient turbulence intensities and thrust coefficient effects. *J. Wind Eng. Ind. Aerodyn.* **2018**, *177*, 275–292. [CrossRef]
36. Clifton, A.; Kilcher, L.; Lundquist, J.K.; Fleming, P. Using machine learning to predict wind turbine power output. *Environ. Res. Lett.* **2013**, *8*, 024009. [CrossRef]
37. Wagner, R.; Courtney, M.; Gottschall, J.; Lindelöw-Marsden, P. Accounting for the speed shear in wind turbine power performance measurement. *Wind Energy* **2011**, *14*, 993–1004. [CrossRef]
38. Vahidzadeh, M.; Markfort, C.D. Modified Power Curves for Prediction of Power Output of Wind Farms. *Energies* **2019**, *12*, 1805. [CrossRef]
39. Iowa Environmental Mesonet. Available online: https://mesonet.agron.iastate.edu/ (accessed on 23 January 2020).



© 2020 by the authors. Licensee MDPI, Basel, Switzerland. This article is an open access article distributed under the terms and conditions of the Creative Commons Attribution (CC BY) license (http://creativecommons.org/licenses/by/4.0/).